JOURNAL OF Materials CHEMISTRY

Structural effects of Co and Cr substitution in $LaMnO_{3+\delta}$

Z. El-Fadli,† M. R. Metni,† F. Sapiña, E. Martinez, J. V. Folgado, D. Beltrán and A. Beltrán

Institut de Ciència dels Materials de la Universitat de València, Apartado de Correos 2085, E-46071 València, Spain. E-mail: fernando.sapina@uv.es

Received 6th September 1999, Accepted 29th October 1999

Series of perovskite oxides with the composition $LaMn_{1-x}M_xO_{3+\delta}$ (M = Cr, Co; $0 \leqslant x \leqslant 1$) have been synthesized by thermal treatment of precursors obtained by freeze-drying of acetic acid solutions. The oxides have been characterized by X-ray diffraction, and the Mn^{4+} content and, thus, the oxygen excess, δ, has been determined by redox back-titration. $LaMnO_{3.14}$ and $LaCrO_3$ phases have the rhombohedral-$LaAlO_3$ and the orthorhombic-$GdFeO_3$ structures, respectively. The $LaMn_{1-x}Cr_xO_{3+\delta}$ phases have the rhombohedral structure for $x \leqslant 0.3$, and the orthorhombic structure for $x \geqslant 0.5$. $LaCoO_3$ has, as $LaMnO_{3.14}$, the rhombohedral structure. However, the $LaMn_{1-x}Co_xO_{3+\delta}$ phases have orthorhombic structure for $0.05 \leqslant x \leqslant 0.55$. The evolution of the crystal symmetry has been interpreted by considering the effect of the size of the substituting ion on the capability of the perovskite network to accommodate the oxygen excess (δ).

Introduction

Structural predictions of solid-sate materials using easily obtainable parameters remains an important problem.[1] Such a wise assertion centres the conclusions of Giaquinta and Zur Loye after re-examining the ABO_3 phase diagram, while they highlight that the problem is particularly acute for transition-metal oxides and concerns not only the prediction of structures but also to their rationalization after they are determined. There is no doubt that the perovskite structure, which frequently is referred to as one of the more basic structures in the area of solid-state science,[2] constitutes a case in point. It is usually described as a three-dimensional [BO_3] network resulting from the corner sharing of BO_6 octahedra and the A atoms occupy the large 12-fold coordinated cubo-octahedral cavities. Since the work of Goldschmidt, the structural flexibility of the perovskite network has been related to a so-called tolerance factor, which is defined as

$$t = (A{-}O)/[\sqrt{2}(B{-}O)]$$

where the distances A–O and B–O should be calculated from the sums of tabulated empirical ionic radii, however; there is no clear relation between the calculated t values and the particular experimental distortions through which the structure can alleviate the stresses resulting from mismatches between the equilibrium A–O and B–O bond lengths with regard to the ideal cubic array ($SrTiO_3$, $Fm\bar{3}m$). These distortions are interpreted as a consequence of cooperative rotations of the MO_6 octahedra resulting in orthorhombic ($GdFeO_3$, *Pnma*), rhombohedral ($LaAlO_3$, $R\bar{3}c$) or tetragonal ($BaTiO_3$, *P*4*mm*) structures, among others.[3] In any case, these rotations bend the B–O–B bond angle from 180° to $(180-\phi)^\circ$, and ϕ increases with the mismatch.[4] It is this structural flexibility which allows the perovskite structure to accommodate multiple cation substitutions and different types of vacancies in the different sublattices,[5] what results, in turn, in a diversity of physico-chemical properties and applications.[3]

Insofar the perovskite electronic properties are related to structural details,[6] it seems appropriate to explore structural effects due to modifications of well characterized materials of interest. As discussed below, the $LaMnO_{3+\delta}$ ($0 \leqslant \delta \leqslant 0.18$) perovskites have been thoroughly revisited by Töpfer and Goodenough after discovery of colossal magnetoresistance (CMR) in lanthanide mixed-valence manganates.[7] Starting from a definite composition in this series, namely $LaMnO_{3.14}$, we have synthesized single phase perovskites in the solid solution series $LaMn_{1-x}Cr_xO_{3+\delta}$ and $LaMn_{1-x}Co_xO_{3+\delta}$, and studied the relations between the size and concentration of the substituting cation at B sites, the oxygen excess and the crystal symmetry. Besides the above mentioned interest in phenomena such as CMR, it should be stressed that both manganese and cobalt containing perovskites are very active oxidation catalysts,[8] and those containing manganese and chromium constitute state of the art materials for cathodes and interconnects, respectively, in solid oxide fuel cells.[9]

Experimental

Aqueous solutions of metal acetates with molar nominal compositions La : Mn : M = 1.00 : 1−*x* : *x*, where M = Cr and Co and *x* varies from 0.00 to 1.00 as indicated in Tables 1 and 2, were prepared as follows. The addition of La_2O_3 to a mixture of 100 mL of glacial acetic acid and 20 mL of H_2O led to a suspension, which was gently heated while stirring until a

Table 1 Chemical analysis for samples $LaMn_{1-x}Cr_xO_{3+\delta}$[a]

x	$\%Mn^{4+}$[b]	δ[c]	Proposed stoichiometry[d]
0.00	28	0.14	$La_{0.955}Mn_{0.955}O_3$
0.10	28.5	0.13	$La_{0.958}Mn_{0.863}Cr_{0.095}O_3$
0.20	28	0.11	$La_{0.965}Mn_{0.772}Cr_{0.193}O_3$
0.30	29	0.10	$La_{0.968}Mn_{0.677}Cr_{0.291}O_3$
0.40	28	0.08	$La_{0.974}Mn_{0.584}Cr_{0.390}O_3$
0.50	28.5	0.07	$La_{0.978}Mn_{0.489}Cr_{0.489}O_3$
0.60	28	0.06	$La_{0.980}Mn_{0.392}Cr_{0.588}O_3$
0.70	—	—	—
0.80	—	—	—
0.90	—	—	—
1.00	—	—	—

[a]Estimated errors in the Mn/La and Cr/La ratios are 0.01. [b]±2%. [c]±0.03. [d]Expressed as $La_{3/(3+\delta)}(Mn_{1-x}M_x)_{3/(3+\delta)}O_3$, which is the correct notation from the structural point of view, taking into account that the oxygen excess is accommodated as cationic vacancies.

†On leave from: Départemente de Chimie, Faculté des Sciences, Université Abdelmalek Essaadi, Tétouan, Maroc.

Table 2 Chemical analysis for samples $LaMn_{1-x}Co_xO_{3+\delta}$[a]

x	$\%Mn^{4+}$ [b]	δ[c]	Proposed stoichiometry[d]
0.05	21	0.10	$La_{0.968}Mn_{0.920}Co_{0.048}O_3$
0.10	19	0.09	$La_{0.971}Mn_{0.874}Co_{0.097}O_3$
0.20	11	0.04	$La_{0.987}Mn_{0.790}Co_{0.197}O_3$
0.30	9.5	0.03	$La_{0.990}Mn_{0.693}Co_{0.297}O_3$
0.40	6.5	0.02	$La_{0.994}Mn_{0.597}Co_{0.397}O_3$
0.50	0.5	0.02	$La_{0.994}Mn_{0.497}Co_{0.497}O_3$
0.60	0.5	0.01	$La_{0.997}Mn_{0.399}Co_{0.598}O_3$
0.70	0.5	0.01	$La_{0.997}Mn_{0.299}Co_{0.698}O_3$
0.80	0.5	0.01	$La_{0.997}Mn_{0.199}Co_{0.798}O_3$
0.90	0.5	0.00	$LaMn_{0.1}Co_{0.9}O_3$
1.00	1.5[e]	0.01	$La_{0.997}Co_{0.997}O_3$

[a]Estimated errors in the Mn/La and Co/La ratios are 0.01. [b]$\pm 2\%$. [c]± 0.03. [d]Expressed as $La_{3/(3+\delta)}(Mn_{1-x}M_x)_{3/(3+\delta)}O_3$, which is the correct notation from the structural point of view, taking into account that the oxygen excess is accommodated as cationic vacancies. [e]$\%Co^{4+}$.

transparent solution is obtained (15 min). After cooling, $Mn(CH_3CO_2)_2{\cdot}4H_2O$ was added and dissolved upon stirring. Then, $Cr(NO_3)_3{\cdot}9H_2O$ or $Co(CH_3CO_2)_2{\cdot}4H_2O$ were added and dissolved upon stirring. The masses of the different reagents were adjusted to give 5 g of perovskite. Droplets of the resulting acetic acid solutions were flash frozen by projection on liquid nitrogen and, then, freeze-dried at a pressure of 10^{-4} atm. In this way, dried solid precursors were obtained as loose powders.

Preliminary investigations have shown that the minimum temperature at which the perovskite phase is obtainable (under air flow) is 700 °C (12 h) for all compositions investigated in this work, and these conditions were thus adopted for thermal treatment of the perovskite precursors. After cooling in the furnace, the samples were ground, pelletized and heated under air at 1100 °C for 48 h.

Metal ratios in the solids were determined by energy dispersive analysis of X-rays (EDAX) on a JEOL JSM 6300 scanning electron microscope collected by an Oxford detector with quantification performed using virtual standards on associated Link-Isis software. The operating voltage was 20 kV, and the energy range for analysis was 0–20 keV. The results indicate that there is no significant deviation from the nominal cationic stoichiometry, which is an advantage of this precursor-based synthetic method that has been previously exploited in other related systems.[10] The mean oxidation state of manganese ions and, thus the oxygen content, was determined by redox back-titration of Fe(II) with potassium dichromate in HCl using a Crison CompacT Titrator. Tables 1 and 2 summarize the results of these analyses.

Powder diffraction patterns were obtained from a Seifert C-3000 θ–θ automated diffractometer, using graphite-monochromated Cu-Kα radiation. To reduce preferred orientation, the samples were dusted through a sieve on the holder surface. Routine patterns for phase identification were collected with a scanning step of 0.08° in 2θ over the angular range 2θ 10–70° with a collection time of 3 s $step^{-1}$. For Rietveld analysis, patterns were collected with a scanning step of 0.02° in 2θ, over a wider angular range (2θ 20–100°), and with a longer acquisition time (>10 s $step^{-1}$) in order to enhance statistics. X-Ray data analyses were performed using the FULLPROF program.[11] Graphical representations of the X-ray powder diffraction patterns were performed using the DRXWin program.[12]

Results

Tables 1 and 2 summarize the results of chemical analysis of the samples. Fig. 1 shows the evolution of the Mn^{4+} content (*i.e.*, the Mn^{4+}/Mn_{total} ratio) upon substitution. As can be seen, the two solid solutions present a very different behaviour from this point of view. For $LaMn_{1-x}Cr_xO_{3+\delta}$, the Mn^{4+} content is practically constant, with a value close to 28%, for $0 \leqslant x \leqslant 0.6$. For values of $x > 0.6$, it was impossible to determine the oxygen content by the method used in this work owing to the great difficulties in dissolving the samples in acidic media. In any case, it should be noted that the $LaCrO_3$ 'end member' composition has been systematically prepared as a non-defective (stoichiometric) perovskite.[13] By contrast, for $LaMn_{1-x}Co_xO_{3+\delta}$, the Mn^{4+} content quickly decreases with x, and becomes practically zero for $x = 0.5$.

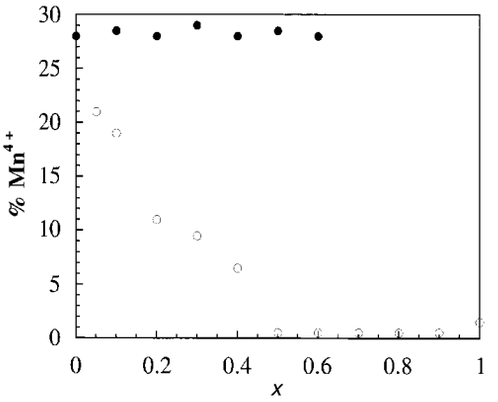

Fig. 1 Evolution of the Mn^{4+} content upon substitution in the $LaMn_{1-x}M_xO_{3+\delta}$ (M = Cr, Co) series; (●) Cr; (○) Co.

Fig. 2 and 3 show the X-ray powder diffraction patterns of selected samples. As can be observed, the diffraction patterns clearly indicate that the structure of the solids in the

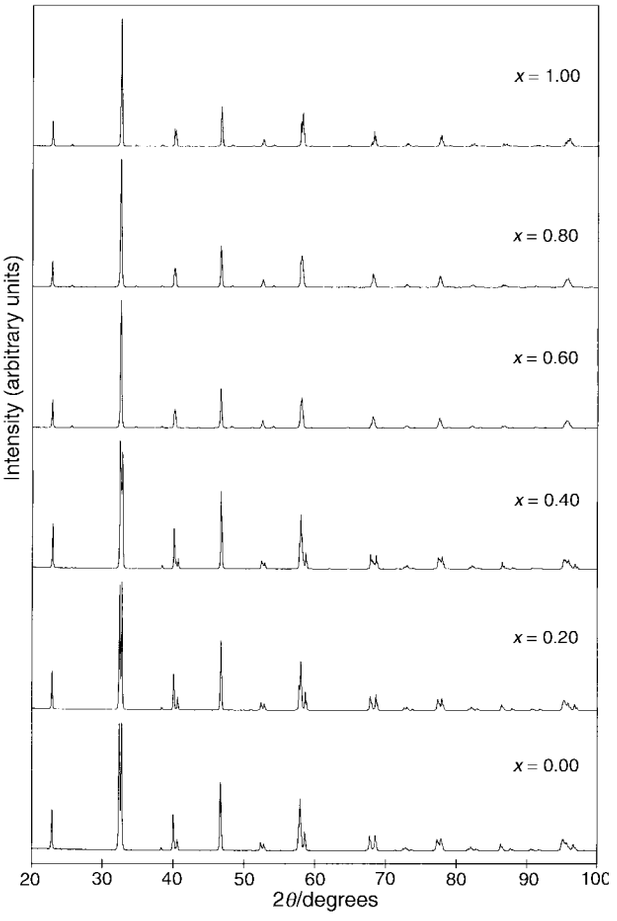

Fig. 2 X-Ray powder diffraction patterns of selected samples in the $LaMn_{1-x}Cr_xO_{3+\delta}$ series.

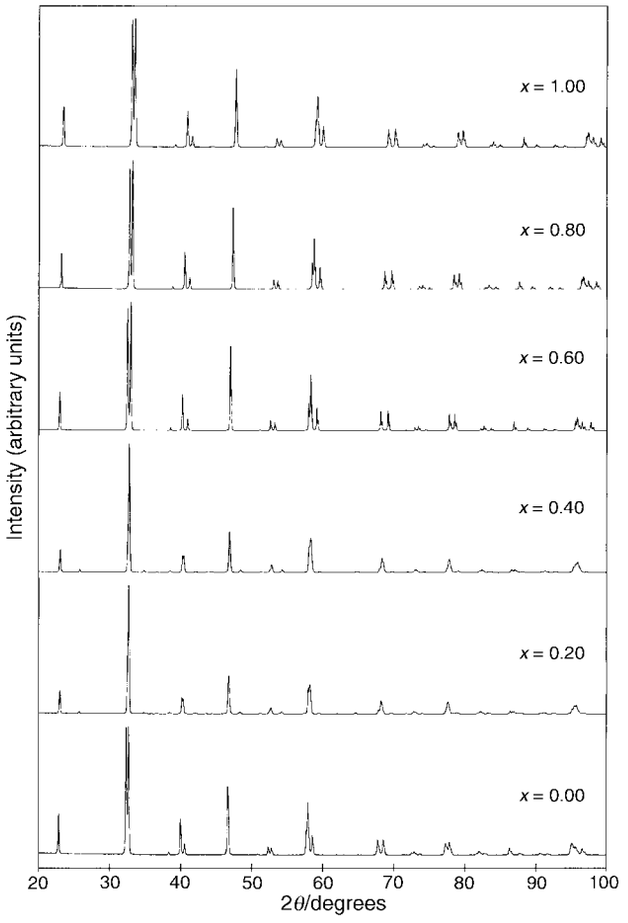

Fig. 3 X-Ray powder diffraction patterns of selected samples in the $LaMn_{1-x}Co_xO_{3+\delta}$ series.

$LaMn_{1-x}M_xO_{3+\delta}$ (M = Cr, Co) series has either orthorhombic symmetry (as $LaCrO_3$)[13] or rhombohedral symmetry (as $LaCoO_3$).[14] Therefore, the structures of the perovskite phases have been refined in space groups $R\bar{3}c$ (in the hexagonal setting) or *Pnma* (for the rhombohedral and orthorhombic samples, respectively) from room temperature X-ray powder diffraction data. The fits were performed using a pseudo-Voigt peak-shape function. In the final runs, the usual profile parameters (scale factors, background coefficients, zero-points, half-width, pseudo-Voigt and asymmetry parameters for the peak-shape) and atomic positions were refined. Isotropic thermal parameters (B) were set at 0.3 and 0.7 Å^2 for metal and oxygen atoms, respectively, and an overall thermal parameter was also refined. In the structural models, Mn and Cr or Co are considered to be randomly distributed in the B sites, and the occupancies of cations at A and B sites were fixed to give the oxygen stoichiometry and metal contents obtained by chemical analysis. Refined structural parameters and residuals, R_p (%), R_{wp} (%), R_B (%) and R_F (%), together with χ^2 values, are listed in Tables 3 and 4. R_p and R_{wp} are the conventional (background corrected) peak only Rietveld profile and weighted profiles residuals while R_B and R_F are the integrated intensity and structure factor residuals, respectively. χ^2 is the square of the goodness-of-fit indicator. Tables 5 and 6 give selected values of bond distances and angles, as well as the values of the normalized volume cell, V/Z (Å^3), and the pseudocubic cell parameter (Å), $\langle a_c \rangle$, calculated as $\langle a_c \rangle = (V/Z)^{1/3}$.

As will be noted, the intermediate $LaMn_{1-x}Cr_xO_{3+\delta}$ compositions have the rhombohedral structure for $x \leqslant 0.3$, whereas the orthorhombic structure is adopted for $x \geqslant 0.5$. Although the aspect of the diffraction pattern corresponding to the $x = 0.4$ sample is similar to that of the rhombohedral samples, the analysis was unsatisfactory. A closer look to the pattern shows the presence of very weak reflections characteristic of orthorhombic symmetry. It should be stressed that the transition between the rhombohedral $R\bar{3}c$ and orthorhombic *Pnma* structures is expected to be first order and, therefore, a two-phase region could exist between the two structural types. The $x = 0.4$ sample seems to lie in this borderline region, a fact that has been previously observed in related systems such as $LaCr_{1-x}Co_xO_3$.[15] The structural behaviour in the $LaMn_{1-x}Co_xO_{3+\delta}$ series is somewhat more complicated. Indeed, the rhombohedral structure corresponding to $LaMnO_{3.14}$ changes to orthorhombic in the range $0.05 \leqslant x \leqslant 0.4$, and then returns to rhombohedral for $0.6 \leqslant x \leqslant 1$.

Fig. 4 shows the variation of the pseudocubic cell parameter, $\langle a_c \rangle$, with x. As can be seen, $\langle a_c \rangle$ remains practically constant along the entire $LaMn_{1-x}Cr_xO_{3+\delta}$ series (it varies by *ca.* 0.18% between the limiting compositions). However, the variation of $\langle a_c \rangle$ is quantitatively (*ca.* 2%) and qualitatively significant along the $LaMn_{1-x}Co_xO_{3+\delta}$ series.

Discussion

As mentioned above, it has become customary to refer the structure and behavior of perovskites to the tolerance factor, t. This notwithstanding, the problem is not simple, especially for transition-metal oxides in which factors others than coulombic or geometric packing effects can significantly contribute to the lattice energies. When revisiting the $LaMnO_{3+\delta}$ ($0 \leqslant \delta \leqslant 0.18$) perovskites, Töpfer and Goodenough pointed out that oxidation of the MnO_3 sublattice, which is accommodated by the formation of cation vacancies, contributes to alleviate the structural stress in the perovskite network.[7] Their room temperature X-ray diffraction results revealed a two-phase region separating an O′-orthorhombic phase stable over $0 \leqslant \delta \leqslant 0.06$ and a rhombohedral phase, stable in the range $0.10 \leqslant \delta \leqslant 0.18$. In the parent stoichiometric $LaMnO_3$ compound, which can be prepared under an inert atmosphere, each Mn^{3+} ion has one strongly antibonding electron, and is Jahn–Teller active. In the space group *Pnma* (non-standard *Pbnm*), the structure can accommodate a static cooperative Jahn–Teller deformation (superimposed on the orthorhombic structure resulting from $t < 1$), with an antiferrodistortive ordering of the elongated MnO_6 octahedra in the *ac* plane.[16] The Mn average radius ($\langle r_{Mn} \rangle$) decreases as the degree of oxidation increases (*i.e.*, with increasing δ): by removing antibonding electrons, the mean equilibrium Mn–O bond length becomes shortened, this leading to t values closer to 1. Thus, the orthorhombicity will decrease with increasing δ (*i.e.*, with increasing the Mn^{4+} content), and the structure changes to the $R\bar{3}c$ rhombohedral phase (in which the static Jahn–Teller deformation is suppressed). As discussed below, although the Töpfer and Goodenough explanations are well founded, some statements are needed to understand the results for the $LaMn_{1-x}M_xO_{3+\delta}$ (M = Cr, Co; $0 \leqslant x \leqslant 1$) perovskites studied in this work.

Let us consider the $LaMnO_{3.14}$ perovskite as the starting point. Its structure is rhombohedral ($R\bar{3}c$), and the calculated value of the pseudocubic cell parameter (Table 3) is very similar to others previously reported for samples with similar compositions.[17] In line with the above, such a value is significantly lower than that corresponding to the stoichiometric $LaMnO_3$ perovskite (represented by an open circle in Fig. 4).[16] There can be no doubt that this effect is mainly due to the presence of a significant proportion of Mn^{4+} (28%) after oxidation of the MnO_3 sublattice. Also, the calculated $\langle a_c \rangle$ values for the $LaCoO_3$ ($R\bar{3}c$ space group) and the $LaCrO_3$ (*Pnma* space group) end compositions are very similar to those previously reported in the literature.[13,14] It is interesting to note

Table 3 Structural data from X-ray powder diffraction studies of $LaMn_{1-x}Cr_xO_{3+\delta}$[a]

Atom	x	y	z
$x=0.0$, $R\bar{3}c$, $a=5.5301(2)$ Å, $c=13.3525(6)$ Å			
$R_p=11.7$, $R_{wp}=15.1$, $R_B=4.49$, $R_F=3.26$, $\chi^2=3.12$			
O	0.5523(11)		
$x=0.2$, $R\bar{3}c$, $a=5.52672(19)$ Å, $c=13.3355(5)$ Å			
$R_p=11.8$, $R_{wp}=15.4$, $R_B=5.28$, $R_F=3.98$, $\chi^2=6.09$			
O	−0.5521(11)		
$x=0.3$, $R\bar{3}c$, $a=5.52452(20)$ Å, $c=13.3308(5)$ Å			
$R_p=12.8$, $R_{wp}=16.4$, $R_B=5.24$, $R_F=3.786$, $\chi^2=5.35$			
O	−0.5525(12)		
$x=0.5$, *Pnma*, $a=5.48407(20)$ Å, $b=7.7716(3)$ Å, $c=5.52436(18)$ Å			
$R_p=10.0$, $R_{wp}=13.0$, $R_B=4.92$, $R_F=4.47$, $\chi^2=3.16$			
La	0.01749(13)		−0.00568(24)
O1	0.4945(16)		0.0645(23)
O2	0.2762(19)	0.0273(15)	0.7270(20)
$x=0.6$, *Pnma*, $a=5.48982(24)$ Å, $b=7.7787(4)$ Å, $c=5.52277(23)$ Å			
$R_p=9.95$, $R_{wp}=13.8$, $R_B=4.29$, $R_F=3.85$, $\chi^2=1.95$			
La	0.02099(14)		−0.0057(3)
O1	0.4919(16)		0.069(3)
O2	0.2776(20)	0.0287(17)	0.7228(20)
$x=0.8$, *Pnma*, $a=5.48835(22)$ Å, $b=7.7783(3)$ Å, $c=5.52132(20)$ Å			
$R_p=9.17$, $R_{wp}=13.3$, $R_B=2.95$, $R_F=3.14$, $\chi^2=1.67$			
La	0.02012(13)		−0.0053(3)
O1	0.4940(16)		0.070(3)
O2	0.2738(21)	0.0285(17)	0.7225(20)
$x=1.0$, *Pnma*, $a=5.47946(14)$ Å, $b=7.75943(19)$ Å, $c=5.51577(13)$ Å			
$R_p=9.98$, $R_{wp}=13.6$, $R_B=4.52$, $R_F=3.77$, $\chi^2=2.14$			
La	0.0195(14)		−0.0051(3)
O1	0.4944(17)		0.066(23)
O2	0.2721(20)	0.0321(13)	0.7273(20)

[a]Space group $R\bar{3}c$, hexagonal setting. La (6a): (0, 0, ¼); Mn, Cr (6b): (0, 0, 0); O (18e): (x, 0, ¼). Space group *Pnma*. La (4c): (x, 1/4, z); Mn, Cr (4b): (0, 0, 1/2); O1 (4c): (x, 1/4, z); O2 (8d) (x, y, z).

that the evolution of the $\langle a_c \rangle$ parameter, $LaCoO_3 < LaCrO_3 < LaMnO_3$, is in agreement with what can expected from the B cationic radii for coordination number six. What should be explained is the structural evolution as manganese is partially replaced in $LaMnO_{3.14}$ by Cr or Co to yield the $LaMn_{1-x}M_xO_{3+\delta}$ (M = Cr, Co) series.

As mentioned above, the $\langle a_c \rangle$ value is practically constant along the entire $LaMn_{1-x}Cr_xO_{3+\delta}$ series (including the $LaMnO_{3.14}$ and $LaCrO_3$ limit compositions), whereas the structure changes from rhombohedral ($LaMnO_{3.14}$, $LaAlO_3$ type) to orthorhombic ($LaCrO_3$, $GdFeO_3$ type) for $x \geqslant 0.5$. The fact that the $\langle a_c \rangle$ values corresponding to $LaMnO_{3.14}$ and $LaCrO_3$ are practically equal indicates that the average effective radius of Mn ions in $LaMnO_{3.14}$ (*i.e.*, when there is 72% Mn^{3+} and 28% Mn^{4+}) is nearly coincident with that of Cr^{3+}. Thus, as far as the Mn^{4+} content (and, therefore, $\langle r_{Mn} \rangle$) remains constant (28%) until, at least, $x=0.6$, we can explain the constancy of the $\langle a_c \rangle$ value in this range of compositions. On the other hand, although we have been not able to determine the Mn^{4+} content values for $x \geqslant 0.7$, the relatively low total manganese content in these perovskites would make negligible (as occurs in practice) any contribution to the $\langle a_c \rangle$ values owing to hypothetical variations in the Mn^{4+} content. In any case, it should be emphasized that the rhombohedral to orthorhombic structural change occurs for $x \geqslant 0.5$, that it to say for a x value for which the Mn^{4+} content (and, therefore, the $\langle r_{Mn} \rangle$ value) is the same that in $LaMnO_{3.14}$ (28%). Hence, we can not associate this structural change with only size effects as

Table 4 Structural data from X-ray powder diffraction studies of $LaMn_{1-x}Co_xO_{3+\delta}$[a]

Atom	x	y	z
$x=0.2$, *Pnma*, $a=5.50764(18)$ Å, $b=7.8015(3)$ Å, $c=5.54492(17)$ Å			
$R_p=10.6$, $R_{wp}=13.7$, $R_B=3.41$, $R_F=3.83$, $\chi^2=1.95$			
La	0.02114(13)		−0.0046(3)
O1	0.4930(17)		0.0825(24)
O2	0.2750(20)	0.0258(15)	0.7238(19)
$x=0.4$, *Pnma*, $a=5.49785(17)$ Å, $b=7.7884(3)$ Å, $c=5.53628(16)$ Å			
$R_p=9.60$, $R_{wp}=13.4$, $R_B=3.51$, $R_F=3.36$, $\chi^2=1.94$			
La	0.02249(13)		−0.00552(24)
O1	0.4927(16)		0.0755(23)
O2	0.2723(21)	0.0310(14)	0.7230(18)
$x=0.6$, $R\bar{3}c$, $a=5.50620(13)$ Å, $c=13.2240(3)$ Å			
$R_p=10.9$, $R_{wp}=15.5$, $R_B=4.32$, $R_F=2.78$, $\chi^2=6.25$			
O	−0.5563(13)		
$x=0.8$, $R\bar{3}c$, $a=5.46870(14)$ Å, $c=13.1497(4)$			
$R_p=10.2$, $R_{wp}=14.1$, $R_B=4.10$, $R_F=2.66$, $\chi^2=5.76$			
O	−0.5519(12)		
$x=1.0$, $R\bar{3}c$, $a=5.44808(12)$ Å, $c=13.1088(3)$			
$R_p=9.75$, $R_{wp}=12.2$, $R_B=3.05$, $R_F=2.04$, $\chi^2=3.24$			
O	−0.5514(9)		

[a]Space group $R\bar{3}c$, hexagonal setting. La (6a): (0, 0, ¼); Mn, Co (6b): (0, 0, 0); O (18e): (x, 0, ¼). Space group *Pnma*. La (4c): (x, 1/4, z); Mn, Co (4b): (0, 0, 1/2); O1 (4c): (x, 1/4, z); O2 (8d) (x, y, z).

Table 5 Selected bond distances (Å) and angles (°), and cell parameters (Å) for pseudocubic cells of $LaMn_{1-x}Cr_xO_{3+\delta}$

	x						
	0.0	0.2	0.3	0.5	0.6	0.8	1.0
La–O(1)	2.476(4) × 3	2.475(4) × 3	2.472(5) × 3	2.440(13 × 1	2.416(16) × 1	2.407(16) × 1	2.425(12) × 1
	2.754(2) × 3	2.751(2) × 3	2.750(3) × 3	2.645(9) × 1	2.618(9) × 1	2.634(9) × 1	2.631(9) × 1
	3.054(4) × 1	3.051(4) × 6	3.052(3) × 6	2.894(9) × 1	2.934(9) × 1	2.918(9) × 1	2.904(9) × 1
				3.090(13) × 1	3.117(16) × 1	3.122(16) × 1	3.098(12) × 1
La–O(2)				2.498(11) × 2	2.487(12) × 2	2.497(12) × 2	2.486(10) × 2
				2.681(11) × 2	2.682(12) × 2	2.677(12) × 2	2.637(10) × 2
				2.753(11) × 2	2.742(12) × 2	2.748(13)| × 2	2.782(10) × 2
				3.100(11) × 2	3.155(12) × 2	3.120(12) × 2	3.117(10) × 2
M–O(1)	1.967(3 × 6	1.966(3) × 6	1.965(4) × 6	1.976(3) × 2	1.982(3) × 2	1.983(3) × 2	1.974(2) × 2
M–O(2)				1.956(11) × 2	1.971(11) × 2	1.954(11) × 2	1.965(11) × 2
				1.978(10) × 2	1.971(11) × 2	1.984(11) × 2	1.971(10) × 2
⟨M–O⟩				1.970(8)	1.975(8)	1.974(8)	1.970(8)
M–O(1)–M	163.1(2)	163.1(3)	163.0(3)	159.1(5)	157.6(3)	157.4(6)	158.6(5)
M–O(2)–M				163(3)	162(3)	163(3)	162(3)
a_c				3.8779	3.8819	3.8809	3.8746
b_c				3.8858	3.8894	3.8892	3.8797
c_c				3.9064	3.9052	3.9042	3.9002
V/Z	58.9392	58.7845	58.7252	58.8640	58.9613	58.9273	58.6293
$\langle a_c \rangle$	3.8917	3.8883	3.8869	3.8900	3.8921	3.8914	3.8848

characterized by the tolerance factor. From the available data, it would appear as if the perovskites in the $LaMn_{1-x}Cr_xO_{3+\delta}$ series are in a borderline region between the rhombohedral and orthorhombic structures as a consequence of cationic size effects. If so, other factors could make the structure evolve in one or other directions. While maintaining the Mn^{4+} content in $LaMn_{1-x}Cr_xO_{3+\delta}$ perovskites, what is decreasing as x increases is the δ value, *i. e.* the cationic vacancy concentration. In practice, it is found that the rhombohedral structure is adopted for relatively high cationic vacancy concentrations (small x values): as far as the disorder associated with the presence of vacancies favours the more symmetrical structure, it seems that such a contribution is sufficient to stabilize the rhombohedral structure under these conditions.

On the other hand, the situation is substantially different in the $LaMn_{1-x}Co_xO_{3+\delta}$ series. Indeed, the $\langle a_c \rangle$ value initially increases as manganese is replaced by cobalt, but then falls markedly as substitution progresses. Also, the Mn^{4+} content (and the δ value) quickly decrease with x (and becomes negligible for $x \geqslant 0.5$), whereas the rhombohedral structure of $LaMnO_{3.14}$ changes immediately ($x = 0.05$) to the orthorhombic structure, and returns to rhombohedral for $x \geqslant 0.5$ ($\delta \approx 0$). In short, from the structural point of view, the behaviour along the $LaMn_{1-x}Co_xO_{3+\delta}$ series is the opposite of that observed in the $LaMn_{1-x}Cr_xO_{3+\delta}$ series, which can be easily understood using the same rationale as above. In effect, the initial increase of $\langle a_c \rangle$ reflects the rapid decrease in the Mn^{4+} content, which would result in a comparatively high decrease in t.

Simultaneously, the disorder contribution (δ value, cationic vacancy concentration) becomes reduced. So, for low x values, the factors that contribute to stabilize the rhombohedral structure in the chromium series do not apply for the cobalt perovskites, and a structural transition occurs. Only when the substitution of manganese by the smaller cobalt ions is high enough ($x \geqslant 0.5$), does the decrease of the effective radius of the B cations (and, thus, the increase of t) allow the stabilization of the rhombohedral structure.

From all the above, we can state that the empirical structural effects due to manganese substitution in $LaMnO_{3+\delta}$ to give $LaMn_{1-x}M_xO_{3+\delta}$ (M = Cr, Co; $0 \leqslant x \leqslant 1$) perovskites can be simply rationalized mainly in terms of size effects, the key variable being the average radius of cations at B positions. These $\langle r_B \rangle$ values have to be considered, however, to depend on both the Mn^{4+} content and, obviously, on the concentration and size of the manganese-substituting cations (Cr or Co). In fact, a close observation of Tables 5 and 6 show that the

Table 6 Selected bond distances (Å) and angles (°), and cell parameters (Å) for pseudocubic cells of $LaMn_{1-x}Co_xO_{3+\delta}$

	x				
	0.2	0.4	0.6	0.8	1.0
La–O(1)	2.346(13)x1	2.387(13) × 1	2.443(5) × 3	2.450(4) × 3	2.444(3) × 3
	2.643(9)x1	2.624(9) × 1	2.735(x) × 6	2.716(2) × 6	2.702(2) × 6
	2.949(9) × 1	2.947(9) × 1	3.063(5) × 3	3.018(4) × 3	3.004(3) × 3
	3.208(14) × 1	3.160(13) × 1			
La–O(2)	2.525(11) × 2	2.500(11) × 2			
	2.699(11) × 2	2.656(11) × 2			
	2.737(11) × 2	2.768(11) × 2			
	2.117(11) × 2	3.141(11) × 2			
M–O(1)	1.968(11) × 2	1.956(11) × 2	1.959(4) × 6	1.943(3) × 6	1.935(2) × 6
M–O(2)	1.981(11) × 2	1.992(3) × 2			
	2.004(3) × 2	1.994(10) × 2			
⟨M–O⟩	1.984(8)	1.981(8)			
M–O(1)–M	153.5(5)	155.7(5)	161.8(3)	163.2(3)	163.4(2)
M–O(2)–M	163(3)	163(3)			
a_c	3.8945	3.8876			
b_c	3.9008	3.8942			
c_c	3.9208	3.9147			
V/Z	59.5635	59.2650	57.8688	56.7625	56.1603
$\langle a_c \rangle$	3.9054	3.8988	3.8680	3.8431	3.8295

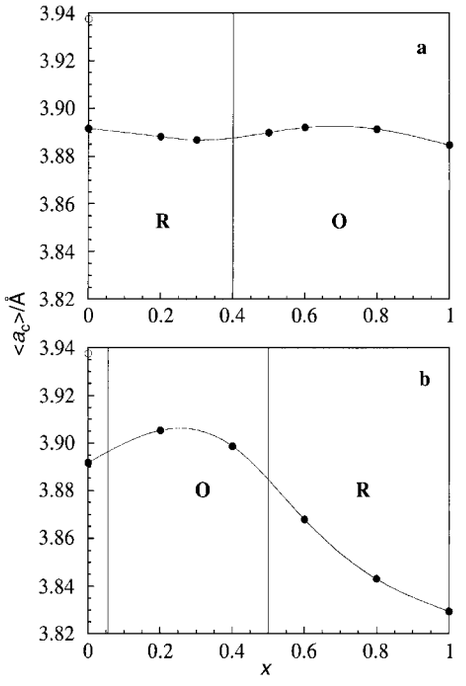

Fig. 4 Evolution of the pseudo-cubic cell parameter, $\langle a_c \rangle$, upon substitution in the $LaMn_{1-x}M_xO_{3+\delta}$ (M = Cr, Co) series. The open circle represents the value of $\langle a_c \rangle$ for stoichiometric $LaMnO_3$: (a) Cr and (b) Co.

refined values of the mean M–O distance further support such average site arguments. These size effects are clearly reflected by the experimental $\langle a_c \rangle$ values, and it is interesting that an eye-guide line at $\langle a_c \rangle \approx 3.88$ Å in Fig. 4 delimits rather accurately the orthorhombic and rhombohedral structural zones for all the compositions in the $LaMn_{1-x}M_xO_{3+\delta}$ (M = Cr, Co) series, except for the rhombohedral region appearing in the chromium series for low x values. It is this last fact which allows us to emphasize the structural relevance of the disorder owing to the presence of cationic vacancies.[18] This notwithstanding, inasmuch as the concentration of cationic vacancies depends on the Mn^{4+} content (which, in turn, influences the $\langle r_B \rangle$ value, and so on), a fundamental question to be answered concerns the reasons making the behavior of the chromium and cobalt series with of the variation of the Mn^{4+} content so different.

Let us advance a tentative approach. The introduction of an oxygen excess in the stoichiometric $LaMnO_3$ perovskite is not a thermodynamically simple process. It implies several free energy contributions: those associated to the generation of A and B cationic vacancies, and those involved in the Mn^{3+} to Mn^{4+} oxidation itself (without prejudice to bond stress alleviation arising from concomitant lowering in the $\langle r_B \rangle$ value). So, when thinking about the accessibility of the Mn^{4+} state after manganese substitution yielding the $LaMn_{1-x}M_xO_{3+\delta}$ (M = Cr, Co) perovskites, we must consider the influence of the substituting cation (Cr^{3+} or Co^{3+}) on factors such as the above. As we are working over the entire compositional series ($0 \leqslant x \leqslant 1$), it seems reasonable to assume that the main parameter that differentiates between the chromium and cobalt series is the difference in cationic radius (Cr^{3+}, 75.5 pm; Co^{3+}, 68.5 pm; Mn^{3+}, 78.5 pm),[19] given that this size dissimilarity influences $\langle r_B \rangle$, and, therefore, affects in different ways the structural stress for a given degree of substitution (x value). Let us consider again the rhombohedral $LaMnO_{3.14}$ perovskite as the starting point. As noted above, the $\langle r_{Mn} \rangle$ value in this compound is nearly coincident with $r(Cr^{3+})$. Then, relating size effects to the structural stress, replacing manganese by chromium has no consequence. In this sense, there is no sound reason for altering the equilibrium 'state' found in the starting product. Hence, the Mn^{3+} to Mn^{4+} oxidation process should be equally favoured in $LaMn_{1-x}Cr_xO_{3+\delta}$ as in $LaMnO_{3.14}$, and it would be essentially driven by the free energy lowering relating to disorder and the lessening of the structural stress associated with oxidation. This situation drastically changes for the cobalt series. The radius of Co^{3+} is significantly lower than $\langle r_{Mn} \rangle$ in $LaMnO_{3.14}$ and the introduction of a comparatively small cation in the lattice implies a lowering of the $\langle r_B \rangle$ value, *i.e.* a reduction in the structural stress due to size effects. As the structural stress is decreased upon substituting cobalt for manganese, the energy lowering related with oxidation also decreases and, therefore, oxidation should be less favoured in the cobalt series in comparison to the chromium series.

Concluding remarks

Transition-metal perovskite oxides constitute one of the most important family of materials. Many are found to be useful in technological applications, a consequence of their wide spectrum of physical properties resulting from the structural flexibility of the perovskite network. As far as structural details in these materials appear linked to particular electronic behaviour, it is worth investigating effects influencing their crystal symmetry. The different behaviours found for the $LaMn_{1-x}M_xO_{3+\delta}$ (M = Cr, Co; $0 \leqslant x \leqslant 1$) series depending on the nature of the entering cation M, reveal the structural relevance of the introduced disorder due to the presence of cationic vacancies, with the effect of the size of the substituting ion on the oxidation potential of the MnO_3 sublattice being of note.

Acknowledgements

The research in Valencia was supported by the Spanish Comisión Interministerial de Ciencia y Tecnología (CICYT, MAT96-1037 and MAT96-0688). Z. El-F. is grateful to the Instituto de Cooperación con el Mundo Arabe (Agencia Española de Cooperación Internacional) and the Universidad de Valencia for grants. The SCSIE of the Universitat de València is acknowledged for X-ray diffraction and analytical facilities.

References

1 D. M. Giaquinta and H. C. Zur Loye, *Chem. Mater.*, 1994, **6**, 365.
2 J. Darriet and M. A. Subramanian, *J. Mater. Chem.*, 1995, **5**, 543.
3 F. S. Galasso, *Perovskites and High T_c Superconductors*, Gordon and Breach Science Publishers, New York, 1990.
4 J. B. Goodenough, *J. Appl. Phys.*, 1997, **81**, 5330.
5 C. M. R. Rao and J. Gopalakrishnan, in *New Directions in Solid State Chemistry*, Cambridge University Press, Cambridge, 1986.
6 J. Vergara, R. J. Ortega-Hertogs, V. Madurga, F. Sapiña, Z. El-Fadli, E. Martinez, A. Beltrán and K. V. Rao, *Phys. Rev. B: Condens. Matter*, 1999, **60**, 1127.
7 J. Töpfer and J. B. Goodenough, *J. Solid State Chem.*, 1997, **130**, 117; J. Töpfer and J. B. Goodenough, *Chem. Mater.*, 1997, **9**, 1467.
8 *Properties and Applications of Perovskite-Type Oxides*, ed. L. J. Tejuca and J. L. G. Fierro, Dekker, New York, 1993.
9 N. Q. Minh, *J. Am. Ceram. Soc.*, 1993, **76**, 563 and references therein.
10 Y. Ng-Lee, F. Sapiña, E. Martinez-Tamayo, J. V. Folgado, R. Ibañez, D. Beltrán, F. Lloret and A. Segura, *J. Mater. Chem.*, 1997, **7**, 1905; T. Boix, F. Sapiña, Z. El-Fadli, E. Martinez, A. Beltrán, J. Vergara, R. J. Ortega and K. V. Rao, *Chem. Mater.*, 1998, **19**, 1569; Z. El-Fadli, E. Coret, F. Sapiña, E. Martinez, A. Beltrán, D. Beltrán and F. Lloret, *J. Mater. Chem.*, 1999, **9**, 1793.
11 J. Rodriguez-Carvajal, FULLPROF: A Program for Rietveld Refinement and Pattern Matching Analysis, *Abstracts of the Satellite Meeting on Powder Diffraction of the XV Congress of the IUCr*, Toulouse, France, 1990, p. 127.
12 V. Primo, DRXWin & CreaFit version 2.0: graphical and

analytical tools for powder XRD patterns, *Powder Diffrac.*, 1999, **14**, 70.
13 C. P. Khattak and D. E. Cox, *Mater. Res. Bull.*, 1977, **12**, 236; H. Taguchi, M. Nagao and Y. Takeda, *J. Solid State Chem.*, 1995, **114**, 236; M. Stojanovic, R. G. Haverkramp, C. A. Mims, H. Moudallal and A. J. Jacobson, *J. Catal.*, 1997, **165**, 315.
14 G. Thornton, B. C. Tofield and A. W. Hewat, *J. Solid State Chem.*, 1986, **61**, 301.
15 B. Gilbu Tilset, H. Fjellvag and A. Kjekshus, *Acta Chem. Scand.*, 1994, **48**, 37.
16 J. B. A. A. Elemans, B. Van Laar, K. R. van der Veen and B. O. Loopstra, *J. Solid State Chem.*, 1971, **3**, 238; P. Norby, E. Krogh Andersen and N. H. Andersen, *J. Solid State Chem.*, 1995, **119**, 191; J. A. M. van Roosmalen, P. A. van Vlaanderen, E. H. P. Cordfunke, W. L. Ijdo and D. J. W. Ijdo, *J. Solid State Chem.*, 1995, **114**, 516.
17 J. A. M. van Roosmalen, E. H. P. Cordfunke, R. B. Helmholdt and H. W. Zandenberg, *J. Solid State Chem.*, 1994, **110**, 100.
18 We obviate here the disorder effects due to substitution itself, which will vary analogously with x regardless the substituting cation be Cr or Co.
19 R. D. Shannon, *Acta Crystallogr., Sect. A*, 1976, **32**, 751.

Paper a907173c